

ORIGINAL PAPER

Determination of supermassive black hole spins in local active galactic nuclei

Accepted for publication in Astronomische Nachrichten

M. Yu. Piotrovich^{*1,2} | S. D. Buliga^{1,2} | T. M. Natsvlshvili¹

¹Central Astronomical Observatory at Pulkovo, St.-Petersburg, Russia

²Special Astrophysical Observatory, Nizhnij Arkhyz, Russia

Correspondence

*M. Yu. Piotrovich, Central Astronomical Observatory at Pulkovo, St.-Petersburg, Russia. Email: mpiotrovich@mail.ru

We estimated the radiative efficiency and spin value for a number of local active galactic nuclei with $z < 0.34$ using 3 popular models connecting the radiative efficiency with such parameters of AGNs as mass of supermassive black hole, angle between the line of sight and the axis of the accretion disk and bolometric luminosity. Analysis of the obtained data shown that the spin value decreases with cosmic time, which is in agreement with results of theoretical calculations for low redshift AGNs of other authors. Also we found that the spin value increases with the increasing mass of SMBH and bolometric luminosity. This is the expected result that corresponds to theoretical calculations. Analysis of the distribution of the spin values shown a pronounced peak in the distribution in $0.75 < a < 1.0$ range. $\sim 40\%$ of objects have spin $a > 0.75$ and $\sim 50\%$ of objects have spin $a > 0.5$. This results are in a good agreement with our previous results and with the results of other authors.

KEYWORDS:

galaxies: nuclei, galaxies: active, accretion, accretion disks

1 | INTRODUCTION

Determination of the spin (dimensionless angular momentum) $a = cJ/GM_{\text{BH}}^2$ (where J is the angular momentum, M_{BH} is the mass of the black hole and c is the speed of light) of a supermassive black hole (SMBH) located in the center of the active galactic nucleus (AGN) is one of the important problems of modern astrophysics. It has been reliably established that the spin value plays a key role in the generation of relativistic jets in AGNs; therefore, it is the power of the relativistic jet that is most often used to determine the spin of the SMBH (Daly, 2011). As a rule, the kinetic power of a relativistic jet is obtained by estimating the magnetic field strength near the SMBH event horizon using the Blandford–Znajek generation mechanism (Blandford & Znajek, 1977). Other frequently used mechanisms are the Blandford–Payne mechanism (Blandford

& Payne, 1982) and Garofalo mechanism (Garofalo, Evans, & Sambruna, 2010).

One of the effective methods for obtaining the spin value a is to determine the radiative efficiency $\epsilon(a)$ of the accretion disk, which depends significantly on the spin value of the black hole (Bardeen, Press, & Teukolsky, 1972; Krolik, 2007; Krolik, Hawley, & Hirose, 2007; Novikov & Thorne, 1973). And, in particular, the maximum possible value is $\epsilon \approx 0.324$ (at $a \approx 0.998$) (Thorne, 1974). Radiative efficiency is defined as $\epsilon = L_{\text{bol}}/\dot{M}c^2$, where L_{bol} is the bolometric luminosity of AGN and \dot{M} is the accretion rate.

There are several models (Davis & Laor (2011), Raimundo, Fabian, Vasudevan, Gandhi, & Wu (2012), Du et al. (2014), Trakhtenbrot (2014), Lawther, Vestergaard, Raimundo, & Grupe (2017)) connecting the radiative efficiency with such parameters of AGNs as mass of SMBH M_{BH} , angle between the line of sight and the axis of the accretion disk i and bolometric luminosity L_{bol} , which could be obtained from observations. The goal of our work is to estimate spin values

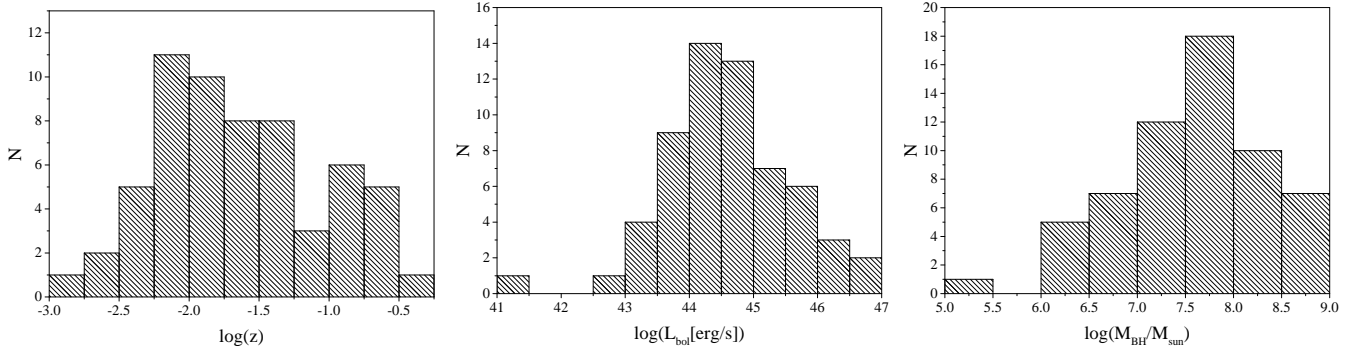


FIGURE 1 Histograms showing the number of objects from our sample with a certain redshift value z , bolometric luminosity value L_{bol} and SMBH mass value M_{BH} .

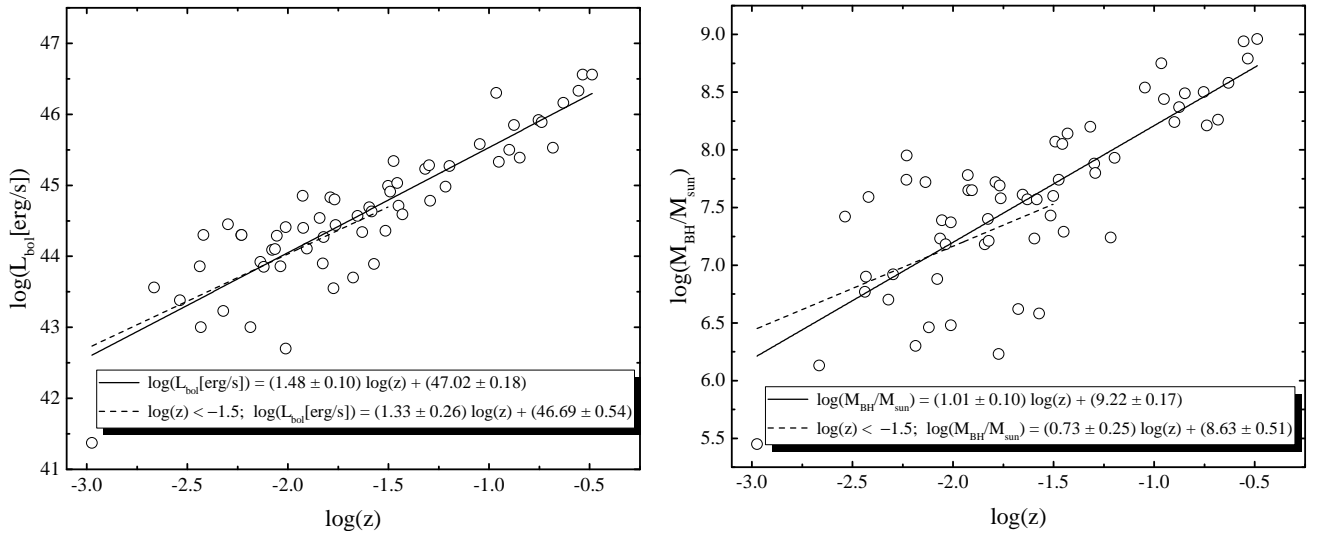


FIGURE 2 Dependences of the bolometric luminosity L_{bol} and the SMBH mass M_{BH} on the cosmological redshift z for our sample.

of SMBHs in AGNs based on this models and the available observational data.

In our work we are using the sample consisted of 111 Seyfert galaxies of the first, second and intermediate types from Marin (2016). We choose the objects from Marin (2016) because for all of this objects Shakura-Sunyaev model (Shakura & Sunyaev, 1973) of a geometrically thin, optically thick accretion disk can be used. And all methods for calculating radiative efficiency used in our paper assume this disk model.

2 | VETTING OF THE INITIAL DATA

First, we will vet the initial data from Marin (2016).

Fig. 1 show distribution of objects by the redshift, mass and bolometric luminosity. The redshift distribution shows an

increase at small z , associated with an increase in the number of objects with increasing distance, and then the number of objects begins to decrease, which is apparently associated with the selection effect, since at large distances the number of objects, which brightness makes it possible to confidently determine their physical parameters, decreases. However, we can see that mass and luminosity distributions have a normal form with a peak in the region of the known mean value of the parameters and thus have no visible manifestations of the selection effect, which could arise because among distant objects we could primarily observe the brightest ones with the largest mass of the central SMBH.

Fig. 2 demonstrate dependences of bolometric luminosity and SMBH mass on redshift. In order to test the possible influence of selection effect on this dependences we make two linear fittings: for all objects and for nearest objects with $\log z < -1.5$. For bolometric luminosity we have:

TABLE 1 Estimated values of spin for all models: a_1 - Raimundo et al. (2012), a_2 - Trakhtenbrot (2014), a_3 - Du et al. (2014), L_{bol} in [erg/s], i in [deg].

| Object | Type | log(z) | log $\frac{M_{BH}}{M_\odot}$ | log L_{bol} | log l_E | i | a_1 | a_2 | a_3 |
|--------------------|----------|------------|------------------------------|---------------|-----------|------|--------|--------|--------|
| 3C 120 | S1.5 | -1.474 | 7.74 | 45.34 | -0.58 | 22.0 | 0.332 | 0.690 | 0.768 |
| Akn 120 | BLS1 | -1.491 | 8.07 | 44.91 | -1.34 | 42.0 | 0.946 | 0.996 | 0.996 |
| Arp 151 | BLS1 | -1.676 | 6.62 | 43.70 | -1.10 | 25.2 | 0.524 | 0.558 | -0.070 |
| ESO 323-G077 | NLS1 | -1.827 | 7.40 | 43.90 | -1.68 | 45.0 | 0.964 | 0.990 | 0.944 |
| ESO 362-G18 | S1.5 | -1.905 | 7.65 | 44.11 | -1.72 | 53.0 | 0.952 | 0.990 | 0.960 |
| Fairall 9 | BLS1 | -1.317 | 8.20 | 45.23 | -1.15 | 35.0 | 0.936 | 0.996 | 0.998 |
| I Zw1 | NLS1 | -1.216 | 7.24 | 44.98 | -0.44 | 8.0 | -0.402 | 0.026 | 0.084 |
| IC 2560 | S2.0 | -2.011 | 6.48 | 42.70 | -1.96 | 66.0 | 0.778 | 0.768 | – |
| IRAS 13349+2438 | S2.0 | -0.964 | 8.75 | 46.30 | -0.63 | 52.0 | 0.524 | 0.910 | 0.968 |
| K 348-7 | S1.0 | -0.631 | 8.58 | 46.16 | -0.60 | 35.0 | 0.736 | 0.958 | 0.990 |
| LEDA 46718 | S1.5 | -1.767 | 7.69 | 44.80 | -1.07 | 27.0 | 0.836 | 0.944 | 0.938 |
| LEDA 47969 | S1.5 | -2.120 | 6.46 | 43.85 | -0.79 | 34.0 | -0.754 | -0.754 | – |
| Mrk 110 | S1.5 | -1.450 | 7.29 | 44.71 | -0.76 | 37.4 | -0.070 | 0.314 | 0.232 |
| Mrk 279 | BLS1 | -1.514 | 7.43 | 44.36 | -1.25 | 35.0 | 0.836 | 0.926 | 0.874 |
| Mrk 335 | NLS1 | -1.595 | 7.23 | 44.69 | -0.72 | 20.0 | 0.210 | 0.474 | 0.416 |
| Mrk 34 | S2.0 | -1.293 | 7.80 | 44.78 | -1.20 | 65.0 | -0.070 | 0.460 | 0.430 |
| Mrk 348 | S2.0 | -1.823 | 7.21 | 44.27 | -1.12 | 60.0 | -0.506 | -0.038 | -0.452 |
| Mrk 359 | NLS1 | -1.774 | 6.23 | 43.55 | -0.86 | 30.0 | -0.506 | -0.624 | – |
| Mrk 463 | S2.0 | -1.298 | 7.88 | 45.28 | -0.78 | 60.0 | -0.824 | 0.084 | 0.254 |
| Mrk 50 | S1.0 | -1.630 | 7.57 | 44.34 | -1.41 | 9.0 | 0.984 | 1.000 | 0.992 |
| Mrk 509 | BLS1 | -1.456 | 8.05 | 45.03 | -1.20 | 19.0 | 0.970 | 1.000 | – |
| Mrk 573 | S2.0 | -1.762 | 7.58 | 44.44 | -1.32 | 60.0 | 0.400 | 0.682 | 0.568 |
| Mrk 590 | BLS1 | -1.584 | 7.57 | 44.63 | -1.12 | 17.8 | 0.876 | 0.956 | 0.944 |
| Mrk 78 | S2.0 | -1.430 | 8.14 | 44.59 | -1.73 | 60.0 | 0.950 | 0.996 | 0.992 |
| Mrk 79 | BLS1 | -1.654 | 7.61 | 44.57 | -1.22 | 58.0 | 0.332 | 0.660 | 0.580 |
| Mrk 817 | S1.5 | -1.502 | 7.60 | 44.99 | -0.79 | 41.6 | 0.162 | 0.558 | 0.590 |
| Mrk 877 | BLS1 | -0.951 | 8.44 | 45.33 | -1.29 | 20.0 | 0.998 | – | – |
| Mrk 896 | NLS1 | -1.572 | 6.58 | 43.89 | -0.87 | 15.0 | 0.136 | 0.186 | -0.564 |
| NGC 1068 | S2.0 | -2.419 | 7.59 | 44.30 | -1.47 | 70.0 | -0.106 | 0.350 | 0.084 |
| NGC 1320 | S2.0 | -2.036 | 7.18 | 43.86 | -1.50 | 68.0 | -0.106 | 0.210 | -0.564 |
| NGC 1386 | S1.9/2.0 | -2.537 | 7.42 | 43.38 | -2.22 | 81.0 | -0.106 | 0.274 | – |
| NGC 1566 | S1.5 | -2.298 | 6.92 | 44.45 | -0.65 | 30.0 | -0.624 | -0.262 | -0.624 |
| NGC 2992 | S2.0 | -2.137 | 7.72 | 43.92 | -1.98 | 70.0 | 0.828 | 0.938 | 0.816 |
| NGC 3227 | S1.5 | -2.438 | 6.77 | 43.86 | -1.09 | 14.2 | 0.652 | 0.710 | 0.350 |
| NGC 3516 | S1.5 | -2.055 | 7.39 | 44.29 | -1.28 | 26.0 | 0.900 | 0.960 | 0.916 |
| NGC 3783 | S1.5 | -2.011 | 7.37 | 44.41 | -1.14 | 15.0 | 0.854 | 0.934 | 0.894 |
| NGC 4051 | NLS1 | -2.666 | 6.13 | 43.56 | -0.75 | 19.6 | -0.754 | – | – |
| NGC 424 | S2.0 | -1.927 | 7.78 | 44.85 | -1.11 | 69.0 | – | -0.142 | -0.142 |
| NGC 4388 | S2.0 | -2.064 | 7.23 | 44.10 | -1.31 | 60.0 | 0.136 | 0.416 | 0.026 |
| NGC 4395 | S1.8 | -2.975 | 5.45 | 41.37 | -2.26 | 15.0 | – | – | 0.084 |
| NGC 4507 | S1.9/2.0 | -1.924 | 7.65 | 44.40 | -1.43 | 47.0 | 0.882 | 0.962 | 0.932 |
| NGC 4593 | BLS1 | -2.079 | 6.88 | 44.09 | -0.97 | 21.6 | 0.446 | 0.568 | 0.254 |
| NGC 4941 | S2.0 | -2.433 | 6.90 | 43.00 | -2.08 | 70.0 | 0.796 | 0.842 | -0.070 |
| NGC 5506 | NLS1 | -2.230 | 7.95 | 44.30 | -1.83 | 80.0 | -0.824 | 0.084 | -0.262 |
| NGC 5548 | S1.5 | -1.789 | 7.72 | 44.83 | -1.07 | 47.3 | 0.568 | 0.812 | 0.804 |
| NGC 7213 | LINER | -2.231 | 7.74 | 44.30 | -1.62 | 21.0 | 1.000 | – | – |
| NGC 7314 | S1.9 | -2.321 | 6.70 | 43.23 | -1.65 | 42.0 | 0.922 | 0.936 | 0.536 |
| PG 0026+129 | NLS1 | -0.848 | 8.49 | 45.39 | -1.28 | 43.0 | 0.972 | – | – |
| PG 1302-102 | S1.0 | -0.555 | 8.94 | 46.33 | -0.79 | 32.0 | 0.954 | – | – |
| PG 1411+442 | BLS1 | -1.046 | 8.54 | 45.58 | -1.14 | 14.0 | 0.994 | – | – |
| PG 1435-067 | BLS1 | -0.900 | 8.24 | 45.50 | -0.92 | 38.0 | 0.808 | 0.964 | 0.982 |
| PG 1626+554 | BLS1 | -0.876 | 8.37 | 45.85 | -0.70 | 31.0 | 0.768 | 0.956 | 0.984 |
| PG 1700+518 | NLS1 | -0.535 | 8.79 | 46.56 | -0.41 | 43.0 | 0.524 | 0.914 | 0.974 |
| PG 2251+113 | S1.0 | -0.488 | 8.96 | 46.56 | -0.58 | 67.0 | -0.452 | 0.626 | 0.824 |
| RBS 1124 | BLS1 | -0.682 | 8.26 | 45.53 | -0.91 | 66.0 | -0.452 | 0.416 | 0.568 |
| Swift J2127.4+5654 | NLS1 | -1.842 | 7.18 | 44.54 | -0.82 | 49.0 | -0.686 | -0.180 | -0.402 |
| Ton 1388 | S1.0 | -0.753 | 8.50 | 45.92 | -0.76 | 39.0 | 0.782 | 0.966 | 0.990 |
| Ton 1542 | BLS1 | -1.197 | 7.93 | 45.27 | -0.84 | 28.0 | 0.724 | 0.912 | 0.938 |
| Ton 1565 | S1.0 | -0.738 | 8.21 | 45.89 | -0.50 | 37.0 | 0.314 | 0.768 | 0.874 |
| UGC 6728 | S1.0 | -2.186 | 6.30 | 43.00 | -1.48 | 55.0 | 0.416 | 0.350 | – |

$\log L_{bol}[\text{erg/s}] = (1.48 \pm 0.10) \log z + (47.02 \pm 0.18)$ for all objects and $\log L_{bol}[\text{erg/s}] = (1.33 \pm 0.26) \log z + (46.69 \pm 0.54)$ for objects with $\log z < -1.5$. For SMBH mass we have: $\log M_{BH}/M_{\text{sun}} = (1.01 \pm 0.10) \log z + (9.22 \pm 0.17)$ for all

objects and $\log M_{BH}/M_{\text{sun}} = (0.73 \pm 0.25) \log z + (8.63 \pm 0.51)$ for objects with $\log z < -1.5$. In both cases the fittings are close within a margin of error. Thus we can conclude that influence of selection effect is relatively weak.

3 | ESTIMATIONS OF RADIATIVE EFFICIENCY AND SPIN

We estimated the value of the radiative efficiency ϵ from observational data for a number of local active galaxies. The initial sample consisted of 111 Seyfert galaxies of the first, second and intermediate types from Marin (2016). The masses of SMBHs M_{BH} , the bolometric luminosities L_{bol} , and the angles i were all taken from Marin (2016).

In Marin (2016) mass and luminosity values were taken from literature and inclination angles were estimated by Marin through several different methods. Such as X-ray spectroscopy, IR spectroscopy, narrow line region (NLR) spectroscopy and other methods. Admittedly, all of these methods have their drawbacks, but at the moment, unfortunately, there is no absolutely reliable method.

There are number of models, that allow us to estimate the radiative efficiency ϵ from this parameters (Davis & Laor (2011), Raimundo et al. (2012), Du et al. (2014), Trakhtenbrot (2014), Lawther et al. (2017)). To get relationship between parameters all of this methods use statistical analysis of observational data on AGNs and Shakura-Sunyaev accretion disk model (Shakura & Sunyaev, 1973). The methods of Davis & Laor (2011) and Raimundo et al. (2012) are basically the same. The Lawther et al. (2017) method is a restatement of the Raimundo et al. (2012) method, where Eq.6 in Raimundo et al. (2012) assumes that optical luminosity L_{opt} is measured at 4392 Å, and Eq.4 in Lawther et al. (2017) contains a wavelength scaling factor. So, the estimations was carried out using the following three different enough models (we changed the form of equations from original papers for greater consistency):

1. Raimundo et al. (2012):

$$\epsilon(a) = 0.063 \left(\frac{L_{\text{bol}}}{10^{46} \text{erg/s}} \right)^{0.99} \left(\frac{L_{\text{opt}}}{10^{45} \text{erg/s}} \right)^{-1.5} M_8^{0.89} \mu^{1.5}.$$

2. Trakhtenbrot (2014):

$$\epsilon(a) = 0.073 \left(\frac{L_{\text{bol}}}{10^{46} \text{erg/s}} \right) \left(\frac{\lambda L_{\lambda}}{10^{45} \text{erg/s}} \right)^{-1.5} \left(\frac{\lambda}{5100 \text{Å}} \right)^{-2} M_8 \mu^{1.5}$$

$$\lambda L_{\lambda} = L_{\text{opt}}, \lambda = 4400 \text{Å}.$$

3. Du et al. (2014):

$$\epsilon(a) = 0.105 \left(\frac{L_{\text{bol}}}{10^{46} \text{erg/s}} \right) \left(\frac{L_{5100}}{10^{45} \text{erg/s}} \right)^{-1.5} M_8 \mu^{1.5}.$$

Here L_{5100} is luminosity at 5100 Å, $M_8 = M_{\text{BH}}/(10^8 M_{\odot})$ and $\mu = \cos i$. For third model (Du et al., 2014) we use the Eddington ratio $l_E = L_{\text{bol}}/L_{\text{Edd}}$, where $L_{\text{Edd}} = 1.5 \times 10^{38} M_{\text{BH}}/M_{\odot}$ is the Eddington luminosity.

There is serious problem in defining the bolometric correction factors that are used for obtaining luminosity value at a certain wavelength from bolometric luminosity. In the literature, we can find factors that differ 2-3 times (Cheng et

al., 2019; Duras et al., 2020; Hopkins, Richards, & Hernquist, 2007; Netzer, 2019; Richards et al., 2006). In this work we decided to use for consistency bolometric correction for luminosity at 5100 Å from Richards et al. (2006): $L_{5100} = L_{\text{bol}}/10.3$ and definition of optical luminosity L_{opt} from Hopkins et al. (2007): $L_{\text{bol}}/L_{\text{opt}} = L_{\text{bol}}/L_B = 6.25(L_{\text{bol}}/(10^{10} L_{\odot}))^{-0.37} + 9.0(L_{\text{bol}}/(10^{10} L_{\odot}))^{-0.012}$, $L_B = L(4400 \text{Å})$.

According to Thorne (1974) radiative efficiency should be in the range $0.039 < \epsilon(a) < 0.324$. After calculations, we got 68 objects for which at least one of the models gave a result within these range. The spin value a was determined numerically using the relation (Bardeen et al., 1972):

$$\epsilon(a) = 1 - \frac{R_{\text{ISCO}}^{3/2} - 2R_{\text{ISCO}}^{1/2} + |a|}{R_{\text{ISCO}}^{3/4} (R_{\text{ISCO}}^{3/2} - 3R_{\text{ISCO}}^{1/2} + 2|a|)^{1/2}}, \quad (1)$$

where R_{ISCO} is the radius of the innermost stable circular orbit of a black hole, which is expressed through the spin as follows:

$$R_{\text{ISCO}}(a) = 3 + Z_2 \pm ((3 - Z_1)(3 + Z_1 + 2Z_2))^{1/2},$$

$$Z_1 = 1 + (1 - a^2)^{1/3}((1 + a)^{1/3} + (1 - a)^{1/3}), \quad (2)$$

$$Z_2 = (3a^2 + Z_1^2)^{1/2}.$$

In the expression for $R_{\text{ISCO}}(a)$, the sign “-” is used for prograde ($a \geq 0$), and the sign “+” for retrograde rotation ($a < 0$).

Table 1 presents the results of our calculations of spin a for all three models. Sign “-” means that the value is out of range. Table 1 also shows type of object, cosmological redshift z , mass of SMBH M_{BH} , bolometric luminosity L_{bol} , Eddington ratio l_E and inclination angle i .

4 | RESULTS

4.1 | Results of the first model (Raimundo et al., 2012)

First we analyse the model from Raimundo et al. (2012). The linear fitting of the dependence of the spin on the cosmological redshift for this model (first panel from Fig. 3) gives us: $a_1 = (0.21 \pm 0.14) \log z + (0.71 \pm 0.23)$. The dependence of the spin on the bolometric luminosity (second panel from Fig. 3) gives us: $a_1 = (0.07 \pm 0.09) \log L_{\text{bol}}[\text{erg/s}] - (2.79 \pm 3.86)$. The dependence of the spin on the mass of SMBH (third panel from Fig.3) gives us: $a_1 = (0.27 \pm 0.11) \log M_{\text{BH}}/M_{\odot} - (1.65 \pm 0.81)$.

4.2 | Results of the second model (Trakhtenbrot, 2014)

Here we analyse the model from Trakhtenbrot (2014). The linear fitting of the dependence of the spin on the cosmological redshift for this model (first panel from Fig. 4) gives us:

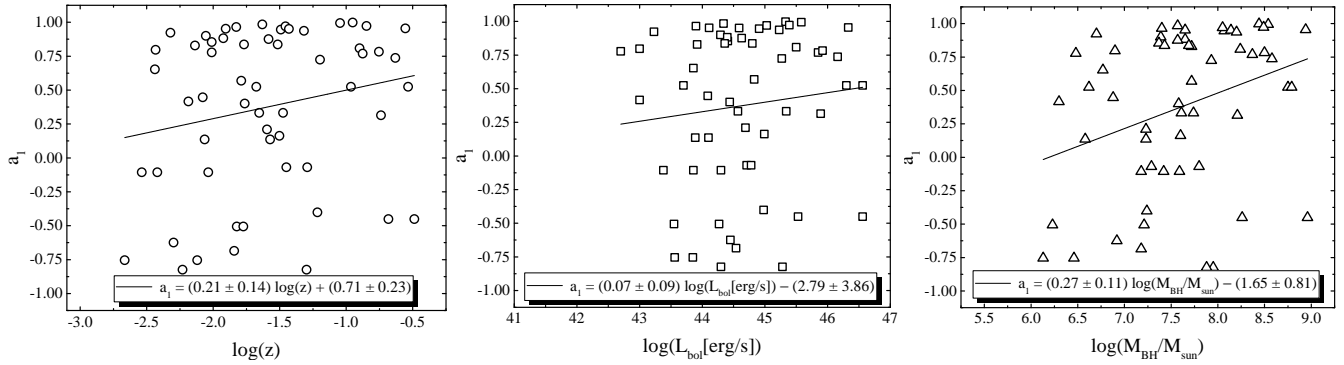


FIGURE 3 Dependence of the spin value a on the redshift z , bolometric luminosity L_{bol} and the SMBH mass M_{BH} for the first model (Raimundo et al., 2012).

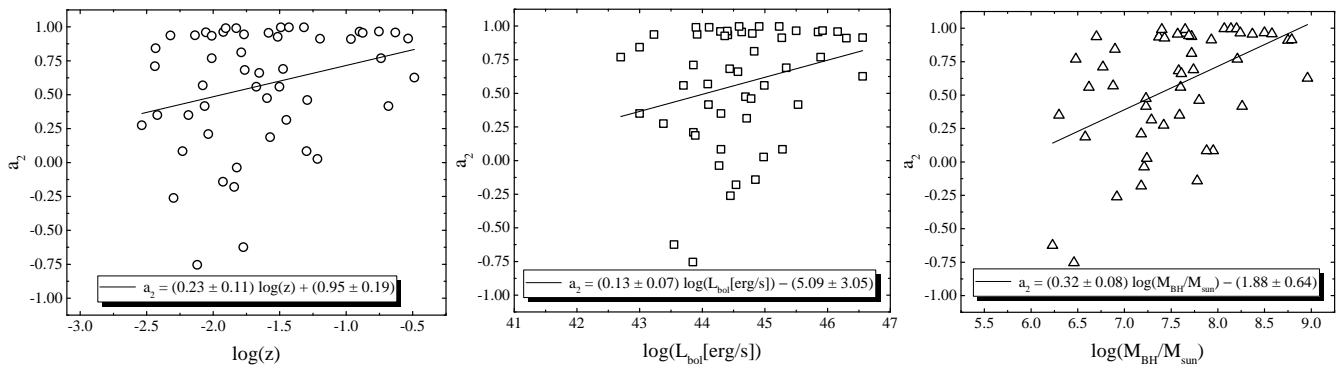


FIGURE 4 Dependence of the spin value a on the redshift z , bolometric luminosity L_{bol} and the SMBH mass M_{BH} for the second model (Trakhtenbrot, 2014).

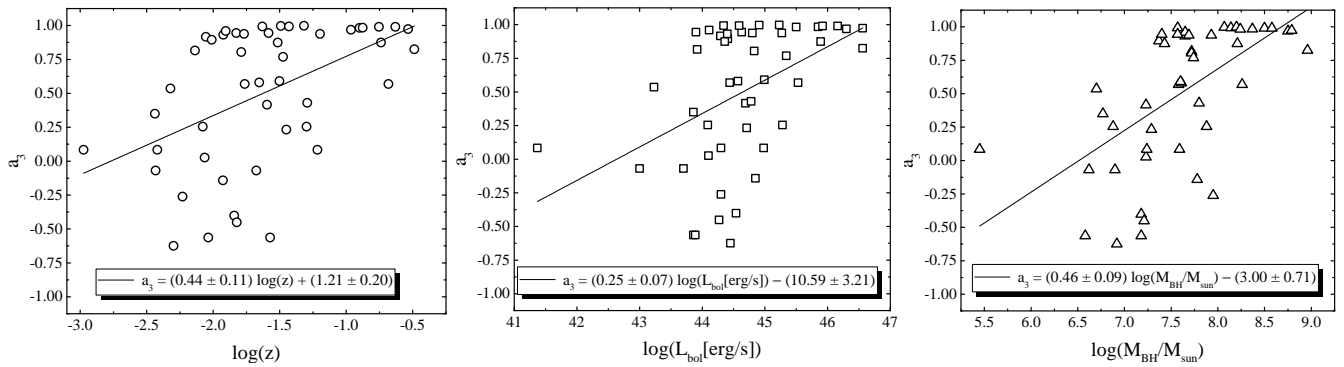


FIGURE 5 Dependence of the spin value a on the redshift z , bolometric luminosity L_{bol} and the SMBH mass M_{BH} for the third model (Du et al., 2014).

$a_2 = (0.23 \pm 0.11) \log z + (0.95 \pm 0.19)$. The dependence of the spin on the bolometric luminosity (second panel from Fig. 4) gives us: $a_2 = (0.13 \pm 0.07) \log L_{\text{bol}}[\text{erg/s}] - (5.09 \pm 3.05)$. The dependence of the spin on the mass of SMBH (third panel from Fig. 4) gives us: $a_2 = (0.32 \pm 0.08) \log M_{\text{BH}}/M_{\odot} - (1.88 \pm 0.64)$.

4.3 | Results of the third model (Du et al., 2014)

And finally we analyse the model from Du et al. (2014). The linear fitting of the dependence of the spin on the cosmological redshift for this model (first panel from Fig. 5) gives us: $a_3 = (0.44 \pm 0.11) \log z + (1.21 \pm 0.20)$. The dependence of the spin on the bolometric luminosity (second panel from Fig. 5) gives

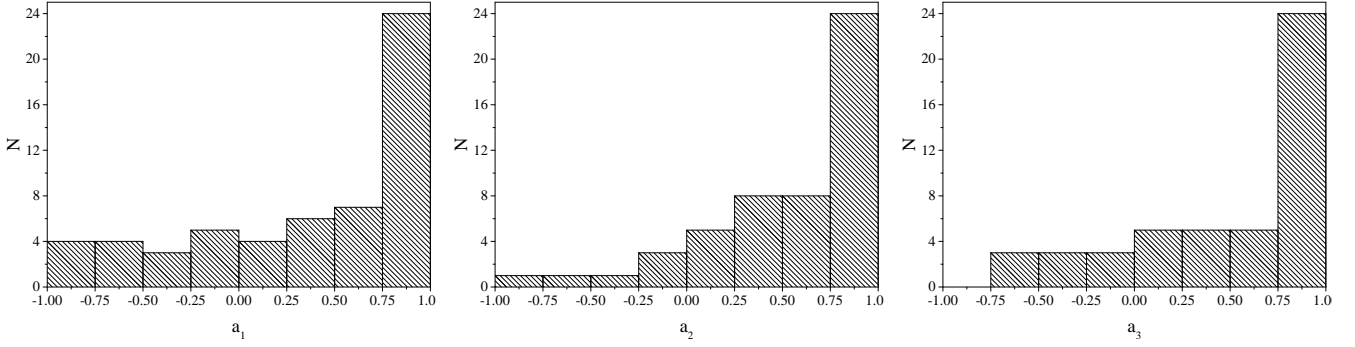


FIGURE 6 Histograms showing the number of objects with a certain spin value a for all individual models: a_1 - Raimundo et al. (2012), a_2 - Trakhtenbrot (2014), a_3 - Du et al. (2014).

us: $a_3 = (0.25 \pm 0.07) \log L_{\text{bol}}[\text{erg/s}] - (10.59 \pm 3.21)$. The dependence of the spin on the mass of SMBH (third panel from Fig. 5) gives us: $a_3 = (0.46 \pm 0.09) \log M_{\text{BH}}/M_{\odot} - (3.00 \pm 0.71)$.

4.4 | Comparison of models and statistical analysis

The linear fitting of the dependence of the spin on the cosmological redshift for all three models shows the same trend and gives close results within a margin of error. However first (Raimundo et al., 2012) and second (Trakhtenbrot, 2014) models have significantly larger errors and their results can rather be considered only as qualitative. We can see that the spin value decreases with cosmic time in all models. This result is in general agreement with results of theoretical calculations for low redshift AGNs. As SMBHs get more massive and galaxies more gas poor, the contribution from binary coalescences to the total BH mass growth increases and tends to decrease the magnitude of spins and change their direction (Dubois, Volonteri, & Silk, 2014; Griffin et al., 2019; Volonteri, Sikora, Lasota, & Merloni, 2013).

Concerning the dependence of the spin on the bolometric luminosity, second (Trakhtenbrot, 2014) and third (Du et al., 2014) models show similar trend. The spin increases with increasing bolometric luminosity. But only the results of the third (Du et al., 2014) model can be considered as quantitative. Results of first (Raimundo et al., 2012) model is uncertain due to large errors. This result is quite expected, because as the spin increases, the radiative efficiency also increases (Bardeen et al., 1972; Krolik, 2007; Krolik et al., 2007; Novikov & Thorne, 1973), which in turn increases luminosity.

Now we consider the dependence of the spin on the mass of SMBH. All models give close results within a margin of error. We can see that the spin value increases with the increasing mass. This result is also in general agreement with the

mentioned above theoretical calculations (Dubois et al., 2014; Griffin et al., 2019; Volonteri et al., 2013).

Fig. 6 presents histograms showing the number of objects with a certain spin value a for all individual models. All histograms show similar distributions. There is a pronounced peak in the distribution in $0.75 < a < 1.0$ range. $\sim 40\%$ of objects have spin $a > 0.75$ and $\sim 50\%$ of objects have spin $a > 0.5$. This results are in a good agreement with our previous results (Afanasiev, Gnedin, Piotrovich, Natsvlshvili, & Buliga, 2018) and with results of other authors (Trakhtenbrot, 2014).

5 | CONCLUSIONS

We estimated the spin value for a sample of 111 AGNs from Marin (2016) using 3 popular models (Du et al., 2014; Raimundo et al., 2012; Trakhtenbrot, 2014) connecting the radiative efficiency (which depends significantly on the spin) with such parameters of AGNs as mass of SMBH M_{BH} , angle between the line of sight and the axis of the accretion disk i and bolometric luminosity L_{bol} .

All three models show qualitatively the same trends in relation to all parameters. But only the results of the third model (Du et al., 2014) can be considered as quantitative. Thus, we can conclude that the third model is the most preferable. However, it should be noted that for more accurate conclusions, an analysis of a larger sample of objects is required.

Analysis of the obtained data shown that the spin value increases with the increasing cosmological redshift, i.e. spin value decreases with cosmic time. For low redshift AGNs, as SMBHs get more massive and galaxies more gas poor, the contribution from binary coalescences to the total BH mass growth increases and tends to decrease the magnitude of spins and change their direction (Dubois et al., 2014; Griffin et al., 2019; Volonteri et al., 2013).

Also we found that the spin value increases with the increasing bolometric luminosity and mass of SMBH. This is the expected result that generally corresponds to theoretical calculations. As the spin increases, the radiative efficiency also increases (Bardeen et al., 1972; Krolik, 2007; Krolik et al., 2007; Novikov & Thorne, 1973), which in turn increases luminosity.

Analysis of the distribution of the mean spin values shown a pronounced peak in the distribution in $0.75 < a < 1.0$ range. $\sim 40\%$ of objects have spin $a > 0.75$ and $\sim 50\%$ of objects have spin $a > 0.5$. This results are in a good agreement with our previous results (Afanasiev et al., 2018) and with the results of other authors (Trakhtenbrot, 2014).

Two serious difficulties in this problem should be noted. First, the presence of several models that give different predictions on the radiative efficiency dependence on other parameters. And, second, the problem of definition of the bolometric correction factors. Both of these problems can be partially solved by analysing the large samples of objects.

ACKNOWLEDGMENTS

This research was supported by the grant of Russian Science Foundation project number 20-12-00030 “Investigation of geometry and kinematics of ionized gas in active galactic nuclei by polarimetry methods”.

REFERENCES

- Afanasiev, V. L., Gnedin, Y. N., Piotrovich, M. Y., Natsvlshvili, T. M., & Buliga, S. D. 2018, *Astronomy Letters*, *44*, 362-369.
- Bardeen, J. M., Press, W. H., & Teukolsky, S. A. 1972, *ApJ*, *178*, 347-370.
- Blandford, R. D., & Payne, D. G. 1982, *MNRAS*, *199*, 883-903.
- Blandford, R. D., & Znajek, R. L. 1977, *MNRAS*, *179*, 433-456.
- Cheng, H., Yuan, W., Liu, H.-Y., Breeveld, A. A., Jin, C., & Liu, B. 2019, *MNRAS*, *487*(3), 3884-3903.
- Daly, R. A. 2011, *MNRAS*, *414*, 1253-1262.
- Davis, S. W., & Laor, A. 2011, *ApJ*, *728*, 98.
- Du, P., Hu, C., Lu, K.-X. et al. 2014, *ApJ*, *782*, 45.
- Dubois, Y., Volonteri, M., & Silk, J. 2014, *MNRAS*, *440*(2), 1590-1606.
- Duras, F., Bongiorno, A., Ricci, F. et al. 2020, *A&A*, *636*, A73.
- Garofalo, D., Evans, D. A., & Sambruna, R. M. 2010, *MNRAS*, *406*, 975-986.
- Griffin, A. J., Lacey, C. G., Gonzalez-Perez, V., Lagos, C. d. P., Baugh, C. M., & Fanidakis, N. 2019, *MNRAS*, *487*(1), 198-227.
- Hopkins, P. F., Richards, G. T., & Hernquist, L. 2007, *ApJ*, *654*(2), 731-753.
- Krolik, J. H. 2007, Making black holes visible: accretion, radiation, and jets. 2007 STScI Spring Symposium on Black Holes p. 309-321.
- Krolik, J. H., Hawley, J. F., & Hirose, S. 2007, The Relationship between Accretion Disks and Jets. *Revista Mexicana de Astronomia y Astrofisica* Vol. 27, p. 1-7.
- Lawther, D., Vestergaard, M., Raimundo, S., & Grupe, D. 2017, *MNRAS*, *467*(4), 4674-4710.
- Marin, F. 2016, *MNRAS*, *460*, 3679-3705.
- Netzer, H. 2019, *MNRAS*, *488*(4), 5185-5191.
- Novikov, I. D., & Thorne, K. S. 1973, Astrophysics of black holes. C. Dewitt & B. S. Dewitt (Eds.), *Black Holes (Les Astres Occlus)* p. 343-450. New York: Gordon and Breach.
- Raimundo, S. I., Fabian, A. C., Vasudevan, R. V., Gandhi, P., & Wu, J. 2012, *MNRAS*, *419*, 2529-2544.
- Richards, G. T., Lacy, M., Storrie-Lombardi, L. J. et al. 2006, *ApJS*, *166*, 470-497.
- Shakura, N. I., & Sunyaev, R. A. 1973, *A&A*, *24*, 337-355.
- Thorne, K. S. 1974, *ApJ*, *191*, 507-520.
- Trakhtenbrot, B. 2014, *ApJ*, *789*, L9.
- Volonteri, M., Sikora, M., Lasota, J. P., & Merloni, A. 2013, *ApJ*, *775*(2), 94.

How cite this article: M.Yu. Piotrovich, S.D. Buliga, and T.M. Natsvlshvili (2021), Determination of supermassive black hole spins in local active galactic nuclei, *Astronomische Nachrichten*, 2021;00:1–6.

How cite this article: M.Yu. Piotrovich, S.D. Buliga, and T.M. Natsvlshvili (2021), Determination of supermassive black hole spins in local active galactic nuclei, *Astronomische Nachrichten*, 2021;00:1–6.